Self-Consistent Numerical 1D/3D Hybrid Modeling of Radio-Frequency Ion Thrusters

IEPC-2015-408／ISTS-2015-b-408

Presented at Joint Conference of 30th International Symposium on Space Technology and Science,
34th International Electric Propulsion Conference and 6th Nano-satellite Symposium
Hyogo-Kobe, Japan
July 4–10, 2015

Chris Volkmar* and Ubbo Ricklefs†
University of Applied Sciences Giessen, Giessen, 35390, Germany

and

Peter J. Klar‡
University of Giessen, Giessen, 35392, Germany

Abstract: In this paper, we show a numerical model of gridded radio-frequency (RF) ion thrusters. The model consists of a set of self-consistently coupled equations based on conservation of charge, energy, and mass inside the system. Those 1D models are again coupled to a 3D quasi-stationary electromagnetic field solver which offers the opportunity of evaluating arbitrary induction coil and discharge chamber geometries in fairly reasonable simulation time. Several input parameter sets can be computed in parallel due to multi-core implementation. Therefore, the model presented can be regarded as a toolbox for ion thruster engineering purposes and rapid virtual prototyping.

The model predicts electrical parameters such as thruster and plasma impedance as well as propulsive performance data. It is thus possible to use it for finding optimized coil and chamber geometries together with optimized input parameters (coil current, volumetric propellant flow rate, and extraction grid voltages) in order to obtain improved mass and electrical efficiency.

To prove the validity of the model, performance mappings experimentally performed on a RIM-4 RF ion thruster assembled at the University of Giessen are used to verify the computed data.

*Research Engineer, Department of Electrical Engineering, chris.volkmar@ei.thm.de
†Professor, Department of Electrical Engineering, ubbo.ricklefs@ei.thm.de
‡Professor, Institute of Experimental Physics I, peter.j.klar@exp1.physik.uni-giessen.de

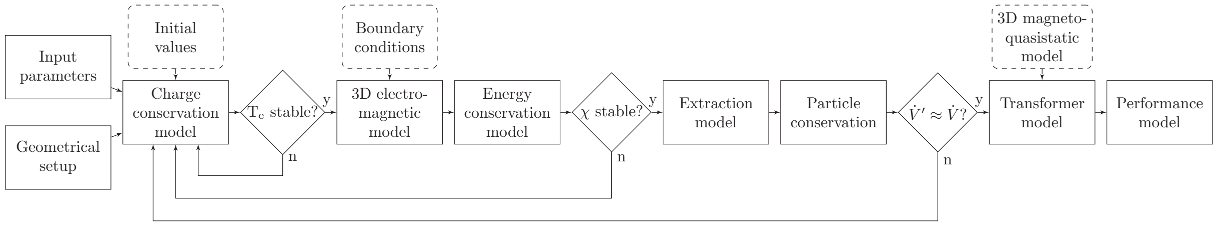

Figure 1. Flow chart of the proposed self-consistent model.

I. Introduction

Radio-frequency (RF) ion thrusters have mainly been used within attitude and orbit control systems (AOCS) for in-orbit satellite stabilization; e.g. north-south station keeping (NSSK), for nearly the last two decades.[1,2] Beside that dominant application, the potential of using RF ion thrusters for orbit raising maneuvers was recognized in the early 2000s during the ARTEMIS mission.[3] Ever since, electric propulsion—headed by Hall and RF ion thrusters—can be regarded as a substantial subsystem of state-of-the-art satellite missions. Despite grid retardation effects, RF ion thrusters illustrate the more promising concept in terms of efficiency and achievable specific impulse.[1] However, since the RF ion thrusters' inductively coupled plasma needs to be supplied by a RF generator (RFG), the whole propulsion system consisting of thruster and generator has to be taken into account when discussing its efficiency. To achieve high overall efficiency $\eta_\Sigma = \eta_{\mathrm{RIT}} \times \eta_{\mathrm{RFG}}$, both thruster efficiency η_{RIT} and generator efficiency η_{RFG} have to be optimized. The optimization of the latter can be realized by adequate control mechanisms and matching networks to ensure low-loss power coupling.

In this paper, we show a numerical model of gridded RF ion thrusters that evaluates thruster performance data, such as specific impulse I_{sp} and thruster efficiency $\eta_{\mathrm{RIT}} = \eta_{\mathrm{el}} \times \eta_m$, where η_{el} denotes the thruster's electrical and η_m its mass efficiency, with respect to its input parameters; i.e, coil current phasor $\widetilde{I}_{\mathrm{c}}$, volumetric propellant flow rate $\dot{V}$, and extraction grid voltages V_{acc} and V_{dec}. Moreover, the impedance loading the generator at its terminals is evaluated for each parameter set. Based on that functionality, the model can be used to perform geometrical modifications of the coil and discharge chamber and the above mentioned input parameters at the same time. The impedance for each structural and input parameter set is furthermore calculated so that the model may be used as an engineering toolbox in virtual prototyping processes.

II. Model Implementation

The presented model comprises three nested one-dimensional conservation equations as well as a three-dimensional electromagnetic field solver that offers the opportunity to handle arbitrary coil and discharge chamber geometries. A flow chart of the implemented algorithm is shown in Fig. 1. A detailed description of the implementation is given in Ref. 4.

The user input is divided into two parts—structural data and signaling parameters. The input signals are based on a real RF ion thruster's signals; i.e., angular RF ω, volumetric flow rate of propellant gas (argon or xenon) $\dot{V}$, coil current phasor $\widetilde{I}_{\mathrm{c}}$, accelerating voltage between screen and acceleration grid V_{acc}, and decelerating voltage between acceleration and ground grid V_{dec}. Those parameters are also shown in Fig. 2 (a) which depicts a schematic image of an electric propulsion system consisting of the actual RF ion thruster and its peripheral actuators; i.e., mass flow controller (MFC), RFG and DC supply, positive high extraction voltage (PHV), and negative high extraction voltage (NHV). For the sake of completeness, a neutralizer is also shown. However, this neutralizer is not taken into account in the numerical model.

Figure 2 (b) shows a numerical implementation of the propulsion system to allow rapid virtual prototyping. It is meant to facilitate the relations between physical system and its software representation. For this purpose, only relevant input and output parameters—that can directly be projected onto the real system—are shown.

The iterative simulation process starts with a calculation of the volume-averaged electron temperature $\mathrm{T_e}$ within the charge conservation model, assuming a Maxwellian energy distribution of electrons and only

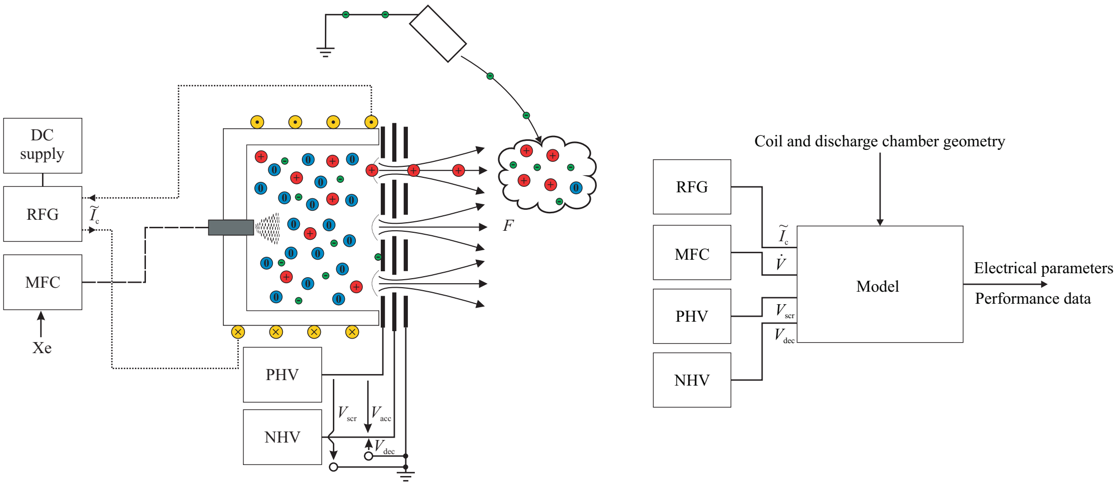

(a) (b)

Figure 2. Schematic of an electric propulsion system consisting of a RF ion thruster and peripheral devices (a). Engineering model for numerical analysis (b).

singly charged ions.[5,6] For convenience, we give the temperatures in volts; i.e., $\mathrm{T_e}\,[\mathrm{V}] = k_\mathrm{B}/e \times T_\mathrm{e}\,[\mathrm{K}]$, with the elementary charge e and Boltzmann's constant k_B. Depending on the shape of the discharge chamber the balance equation that relates volume ionization to wall losses,

$$\frac{K_\mathrm{iz}}{v_\mathrm{B}} = \frac{1}{n_\mathrm{n} d_\mathrm{eff}}, \tag{1}$$

with rate coefficient for electron impact ionization K_iz, Bohm velocity $v_\mathrm{B} = (e\mathrm{T_e}/m_\mathrm{i})^{1/2}$, neutral particle density n_n, effective plasma size d_eff, and ionic mass m_i, is solved for $\mathrm{T_e}$ using Newton's method.[4,7] As mentioned above, a Maxwellian distribution of electrons is assumed; hence, an analytic expression for the rate constant for ionization can be derived:[5]

$$K_\mathrm{iz} = \sigma_0 \overline{v}_\mathrm{e} \left(1 + \frac{2\mathrm{T_e}}{\mathcal{E}_\mathrm{iz}}\right) \exp\left(-\frac{\mathcal{E}_\mathrm{iz}}{\mathrm{T_e}}\right) \tag{2}$$

Here, $\sigma_0 = \pi \left(e/4\pi\epsilon_0 \mathcal{E}_\mathrm{iz}\right)^2$ denotes a constant atomic ionization cross section fraction, with ϵ_0 being the vacuum permittivity and $\mathcal{E}_\mathrm{iz}$ the ionization threshold potential. Furthermore, $\overline{v}_\mathrm{e} = (8e\mathrm{T_e}/\pi m_\mathrm{e})^{1/2}$ denotes the mean Maxwellian electron velocity, with electron mass m_e.

The effective plasma size can be obtained by using the sheath-to-edge density factors given in Ref. 8 that estimate the decrease of electron density towards the discharge chamber walls. This decrease is crucial to satisfy quasi-neutrality within the plasma bulk; i.e., $n_\mathrm{e} \approx n_\mathrm{i}$, due to differing electron and ion flux towards the wall. With h_r and h_p denoting the sheath-to-edge factors for radial and planar walls, respectively, the effective plasma size within a cylindrical discharge chamber calculates to:[5]

$$d_\mathrm{eff} = \frac{1}{2} \frac{r_0 l_0}{r_0 h_p + l_0 h_r} \tag{3}$$

In Eq. (3), l_0 denotes the discharge chamber's axial length and r_0 its inner radius, respectively.

By handling the plasma as a fluid and by defining suitable initial parameters (that are iteratively brought to convergence throughout the simulation task), discharge pressure p, bulk charge carrier density $n_0 = n_\mathrm{e} = n_\mathrm{i}$, neutral gas density n_n, and their corresponding temperatures (in volts) $\mathrm{T_e}$, $\mathrm{T_i}$, and $\mathrm{T_n}$, are related by the ideal gas law:

$$p = n_0 e \left(\mathrm{T_e} + \mathrm{T_i}\right) + n_\mathrm{n} e \mathrm{T_n} \tag{4}$$

Once a stable electron temperature is obtained from Eq. (1), electron-neutral collisional rate constants for elastic and inelastic collisions $K = \langle \sigma \left(v_\mathrm{e}\right) \rangle \overline{v}_\mathrm{e}$, with σ denoting an atomic cross section and v_e the velocity of an incident electron, are obtained by assuming immobile background gas[5] and averaging over a Maxwellian distribution:

$$K = \sqrt{\frac{4e}{\pi m_{\mathrm{e}} \mathrm{T}_{\mathrm{e}}^{3}}} \int \sigma(\mathcal{E})\, \mathcal{E} \exp\left(-\frac{\mathcal{E}}{\mathrm{T}_{\mathrm{e}}}\right) \mathrm{d}\mathcal{E} \tag{5}$$

The xenon cross sections used in this work were obtained by Hayashi in Ref. 9 and taken from a database shown in Ref. 10.

The rate constant for elastic collisions K_{m} can be used to determine the electron-neutral collision frequency for momentum transfer:

$$\nu_{\mathrm{m}} = n_{\mathrm{n}} K_{\mathrm{m}} \tag{6}$$

Furthermore, electron ion-collisions are incorporated, although they seem to play a minor role at low degrees of ionization. The corresponding collision frequency can be approximated by:[11]

$$\nu_{\mathrm{ei}} \approx 2.9 \times 10^{-12} \frac{\mathrm{m}^{3} n_{0} \ln \Lambda}{\mathrm{V}^{-\frac{3}{2}} \mathrm{T}_{\mathrm{e}}^{\frac{3}{2}}} \tag{7}$$

In Eq. (7), the Coulomb logarithm is given by $\ln \Lambda = 23 - 1/2 \times \ln\left(10^{-6} \mathrm{m}^{3} n_{0} / \mathrm{V}^{-3} \mathrm{T}_{\mathrm{e}}^{3}\right)$, as shown in Ref. 11.

Additionally, collisionless stochastic heating is incorporated in terms of a collision frequency ν_{stoc} that describes how electrons, which traverse the electric field layer faster than the duration of one RF cycle, gain net energy from this field.[5,6] Stochastic heating is regarded as the dominant heating mechanism at lower discharge pressures where $\nu_{\mathrm{m}}/\omega < 1$ is satisfied.[5,6] The stochastic collision frequency calculates to

$$\nu_{\mathrm{stoc}} = \frac{\overline{v}_{\mathrm{e}}}{4\delta_{\mathrm{stoc}}}, \tag{8}$$

with the anomalous skin layer depth $\delta_{\mathrm{stoc}} \approx \left(c^{2} \overline{v}_{\mathrm{e}} / \omega \omega_{\mathrm{pe}}^{2}\right)^{3/2}$. In this equation, c denotes the speed of light in vacuum and $\omega_{\mathrm{pe}} = \left(n_{0} e^{2} / m_{\mathrm{e}} \epsilon_{0}\right)^{1/2}$ the bulk electron plasma frequency.

An effective collision frequency can now be obtained by adding the partial contributions:[6]

$$\nu_{\mathrm{m,eff}} = \nu_{\mathrm{m}} + \nu_{\mathrm{ei}} + \nu_{\mathrm{stoc}} \tag{9}$$

Finally, the plasma conductivity can be derived using a Drude model:[5,6]

$$\kappa \approx \frac{\epsilon_{0} \omega_{\mathrm{pe}}^{2}}{\nu_{\mathrm{m,eff}}^{2} + \omega^{2}} \left(\nu_{\mathrm{m,eff}} - \mathrm{i}\omega\right) \tag{10}$$

The approximation is valid in the quasi-stationary electromagnetic regime where only evanescent fields exist and thus the displacement term $\mathrm{i}\omega\epsilon_{0}$ can be neglected.[12] Typical RF ion thrusters work within this regime which corresponds to frequencies covering the single-digit MHz range.[1]

The coupling of the plasma and the induced electromagnetic fields is calculated in the 3D electromagnetic model. Within the quasi-stationary electromagnetic regime the diffusion equation[12]

$$\nabla^{2} \widetilde{\mathbf{A}} - \mathrm{i}\omega \mu_{0} \kappa \widetilde{\mathbf{A}} = -\mu_{0} \widetilde{\mathbf{J}}_{\mathrm{c}}, \tag{11}$$

with vacuum permeability μ_{0} and coil current density $\widetilde{\mathbf{J}}_{\mathrm{c}}$, can be solved for the vector potential $\widetilde{\mathbf{A}}$ which again can be used to obtain the induced electric field $\widetilde{\mathbf{E}}$ and magnetic induction $\widetilde{\mathbf{B}}$, respectively:

$$\widetilde{\mathbf{B}} = \nabla \times \widetilde{\mathbf{A}} \tag{12}$$

$$\widetilde{\mathbf{E}} = -\mathrm{i}\omega \widetilde{\mathbf{A}} \tag{13}$$

Equation (13) is valid in the plasma bulk where $\nabla\Phi = 0$, where Φ denotes the scalar potential.[5,6,12] All occurring vector fields are represented in phasor notation, assuming harmonic fields only. This is a straightforward assumption because the thruster coil is typically driven by a resonant network of high quality. The correspondence between time signals and phasors is given by $E(t) = \mathrm{Re}\left\{\widetilde{\mathbf{E}} \exp(\mathrm{i}\omega t)\right\}$ (exemplified

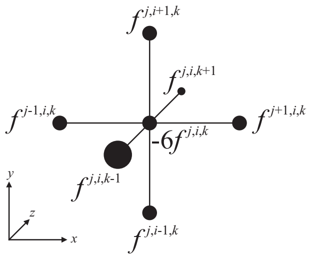

Figure 3. FDM 7-point-stencil of the Laplacian operator in Cartesian coordinates.

by the electric field). The phasor contains information about magnitude E and phase ϕ according to $\widetilde{\mathbf{E}} = \left|\widetilde{\mathbf{E}}\right| \exp(\mathrm{i}\phi) = E \exp(\mathrm{i}\phi)$.

The diffusion equation (11) is solved by a Finite-Difference-Method (FDM) 7-point-stencil for the Laplacian operator ∇^2 in Cartesian coordinates, as shown in Fig. 3. With this functionality, arbitrary coil geometries can be handled. This is regarded as crucial since most numerical models of RF ion thrusters use 2D rotational symmetric methods—or even 1D and 0D methods—which cannot predict the axially induced field components caused by the pitch of the coil.[13−16]

The discrete form of the Laplacian operator in Cartesian coordinates can be derived by a Taylor expansion and subsequent dropping of the discretization error, as shown in Ref. 17:

$$\nabla^2 f^{i,j,k} \approx \frac{1}{h^2}\left(-6f^{i,j,k} + f^{i-1,j,k} + f^{i+1,j,k} + f^{i,j-1,k} + f^{i,j+1,k} + f^{i,j,k-1} + f^{i,j,k+1}\right) \tag{14}$$

In this equation, i, j, and k denote the indexes in x-, y-, and z-direction, respectively, h the node distance between two adjacent mesh nodes, and f an arbitrary function (e.g. the vector potential). Applying this discrete form to Eq. (11) will lead to three systems of linear equations (one per dimension x, y, and z) which have the form

$$(\mathbf{M})\left[\widetilde{A}\right] = \left[\widetilde{b}\right]. \tag{15}$$

Here, $(\mathbf{M})$ denotes a sparsely populated square system matrix of order N^3, where N denotes the number of discrete mesh nodes per dimension. $\left[\widetilde{A}\right]$ and $\left[\widetilde{b}\right]$ denote column vectors containing N^3 unknown complex values of the vector potential at the grid notes and the corresponding set of boundary conditions and source terms, respectively. The vector potential values at each mesh node are obtained by iteratively solving the sparse system matrix using the successive over-relaxation (SOR) method.[18] Methods to solve $\left[\widetilde{A}\right] = (\mathbf{M})^{-1}\left[\widetilde{b}\right]$ directly consume too much memory and are thus not efficient, even if applicable.

With the vector potential, Eq. (13) yields the induced electric field within the simulation domain (inside and outside the plasma / thruster). The electric field, together with the plasma conductivity from Eq. (10), can now be used to determine the induced plasma current density $\widetilde{\mathbf{J}}_{\mathrm{p}}$ by applying Ohm's law:

$$\widetilde{\mathbf{J}}_{\mathrm{p}} = \kappa\widetilde{\mathbf{E}} \tag{16}$$

Since the plasma conductivity is zero outside the plasma; i.e., the discharge chamber, there are only currents induced within the discharge chamber volume. To obtain a lumped-element representation of the discharge—which is the ultimate goal of the model—the current density is volume-averaged using cylindrical coordinates (which is considered useful due to the helical current paths for typical RF ion thruster geometries):[1,7]

$$\widetilde{J}_{\mathrm{p},\varphi} = \widetilde{J}_{\mathrm{p},y}\cos\varphi - \widetilde{J}_{\mathrm{p},x}\sin\varphi \tag{17}$$

$$\widetilde{J}_{\mathrm{p},\rho} = \widetilde{J}_{\mathrm{p},x}\cos\varphi + \widetilde{J}_{\mathrm{p},y}\sin\varphi \tag{18}$$

$$\widetilde{J}_{\mathrm{p},z} = \widetilde{J}_{\mathrm{p},z} \tag{19}$$

The volume-average is taken according to

$$\widetilde{I}_{\mathrm{p}} \approx \left\langle \widetilde{J}_{\mathrm{p},\varphi}\right\rangle_V A_{\mathrm{eff},\varphi} + \left\langle \widetilde{J}_{\mathrm{p},\rho}\right\rangle_V A_{\mathrm{eff},\rho} + \left\langle \widetilde{J}_{\mathrm{p},z}\right\rangle_V A_{\mathrm{eff},z}, \tag{20}$$

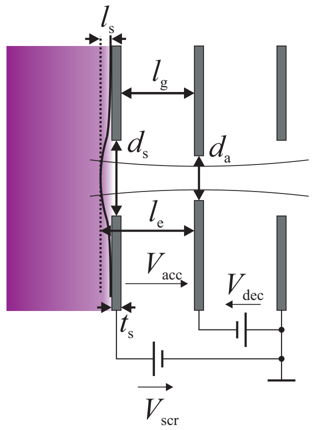

Figure 4. Typical 3-grid extraction system. The effective length l_e takes the inhomogeneity of the plasma sheath into account which arises due to equipotential lines penetrating into the plasma.

where A_{eff} denotes the effective areas the current density components pass through. Those areas are affected by the skin effect that limits the field penetration depth:

$$\delta = \sqrt{\frac{2}{\omega\mu_0 \text{Re}\,\kappa}} \tag{21}$$

This assumption is valid for most stable operating regimes of RF ion thrusters satisfying $\nu_{\text{m,eff}} \geq \omega$ as shown in Refs. 1, 5, and 6. The effective areas calculate to:

$$A_{\text{eff},\varphi} = \delta l_0 \tag{22}$$
$$A_{\text{eff},\rho} = \pi\delta l_0 \tag{23}$$
$$A_{\text{eff},z} = \delta\pi\left(2r_0 - \delta\right) \tag{24}$$

Next, the energy conservation model is called. The absorbed power within the electromagnetic fields inside the discharge volume V is then calculated under consideration of the LHS of Poynting's theorem:[12]

$$P_{\text{abs}} = \frac{1}{2}\iiint_V \text{Re}\left\{\widetilde{\mathbf{J}}_{\text{p}}^{*}\widetilde{\mathbf{E}}\right\} \text{d}\,V \tag{25}$$

Here, * denotes a quantity's complex conjugate. The integration is evaluated using the trapezoidal quadrature rule.[7] For self-consistent treatment between electromagnetic fields and plasma discharge, the absorbed power must equal the sum of losses; i.e., the power lost due to elastic and inelastic collisions given in an energy balance from Ref. 19 and the power lost at the walls due to electron flux $\Gamma_{\text{e}}A_{\text{w}}$:

$$P_{\text{abs}} = \left[n_0\nu_{\text{m,eff}}\frac{3m_{\text{e}}}{m_{\text{n}}}e\left(\text{T}_{\text{e}} - \text{T}_{\text{n}}\right) + \dot{n}_0\left(1 + \frac{\mathcal{E}_{\text{ex}}K_{\text{ex}}}{\mathcal{E}_{\text{iz}}K_{\text{iz}}}\right)e\mathcal{E}_{\text{iz}}\right]V + \left(2e\text{T}_{\text{e}} + eV_{\text{s}}\right)\Gamma_{\text{e}}A_{\text{w}} \tag{26}$$

In Eq. (26), $m_{\text{n}} \approx m_{\text{i}}$ is assumed and $\mathcal{E}_{\text{ex}}$ denotes the threshold potential for excitation from ground state to first excited state. The additional term denotes the power lost to the walls and within the plasma sheath, with sheath voltage V_{s}. The flux density at the walls for Maxwellian electrons furthermore calculates to:[5]

$$\Gamma_{\text{e}} = \frac{1}{4}n_0 h_p \overline{v}_{\text{e}} \exp\left(-\frac{V_{\text{s}}}{\text{T}_{\text{e}}}\right) \tag{27}$$

Equation (26) is iteratively solved for the bulk charge carrier density n_0 using $\dot{n}_0 = n_0 n_{\text{n}} K_{\text{iz}}$ until the degree of ionization $\chi = n_0/\left(n_{\text{n}} + n_0\right)$ converges.

With the upper information, the inductive discharge in the plasma is adequately described. The extraction model is then called to evaluate the ion extraction's influence on the plasma and the propulsive performance of the thruster. Assuming a homogeneous plasma sheath, as depicted in Fig. 4, a modified version of Child-Langmuir's law is used to calculate the amount of extracted current.[20–22] The modified version takes an effective length $l_{\mathrm{e}} = \beta l_{\mathrm{s}} + t_{\mathrm{s}} + l_{\mathrm{g}}$ for ion acceleration into account that contains screen grid thickness t_{s}, inter-grid distance l_{g}, plasma sheath size l_{s}, and a scaling parameter β that is used for compensation of the influence of the plasma meniscus on ion extraction:

$$I_{\mathrm{b}} = \frac{N_{\mathrm{h}} \pi d_{\mathrm{s}}^2 \epsilon_0}{9} \sqrt{\frac{2e}{m_{\mathrm{i}}}} \frac{V_{\mathrm{acc}}^{\frac{3}{2}}}{l_{\mathrm{e}}^2} \tag{28}$$

Here, N_{h} denotes the amount of extraction holes in the extraction system and d_{s} denotes the diameter of the screen grid's extraction holes.

The scaling parameter is found to be a strong function of the extraction system geometry, the amount of extracted ion beam current, and the applied acceleration voltage, respectively. Therefore, it is necessary to define a set point value of extracted ion current and use control mechanisms to iteratively reach the desired output.

To obtain the sheath size l_{s}, the intrinsic extractable ion current density (with floating screen grid) is used. It calculates to

$$J_{\mathrm{p,i}} = e h_p n_0 v_{\mathrm{B}}. \tag{29}$$

The corresponding current is space-charge-limited within the plasma sheath length by the voltage across the sheath V_{s}. Therefore, the unmodified Child-Langmuir's law can be applied:

$$J_{\mathrm{p,i}} = \frac{4\epsilon_0}{9} \sqrt{\frac{2e}{m_{\mathrm{i}}}} \frac{V_{\mathrm{s}}^{\frac{3}{2}}}{l_{\mathrm{s}}^2} \tag{30}$$

Substituting Eq. (29) in Eq. (30), the plasma sheath size is obtained:

$$l_{\mathrm{s}} = \sqrt{\frac{4\epsilon_0}{9} \sqrt{\frac{2e}{m_{\mathrm{i}}}} \frac{V_{\mathrm{s}}^{\frac{3}{2}}}{e h_p n_0 v_{\mathrm{B}}}} \tag{31}$$

Since quasi-neutrality within the bulk forces electron and ion flux densities at the floating walls to be balanced[5]; i.e., $\Gamma_{\mathrm{e}} = \Gamma_{\mathrm{i}}$, the ion flux density at the floating screen grid can be expressed as (with $\Gamma_{\mathrm{i}} = J_{\mathrm{p,i}}/e$):

$$\Gamma_{\mathrm{i}} = h_p n_0 v_{\mathrm{B}} \tag{32}$$

Substituting this with Eq. (27) the voltage across the sheath is obtained:

$$V_{\mathrm{s}} = \mathrm{T_e} \ln\left(\frac{4 v_{\mathrm{B}}}{\overline{v}_{\mathrm{e}}}\right) \tag{33}$$

Setting the plasma potential $\Phi_{\mathrm{p}} = 0$, the wall potential calculates to $\Phi_{\mathrm{w}} = -V_{\mathrm{s}}$. This is due to the walls charging negatively caused by higher electron mobility.[5]

The flux of neutral particles leaving the thruster through the extraction system is obtained using Eq. (27), neglecting the Boltzmann factor due to absence of electric charge:

$$\gamma_{\mathrm{n}} = \frac{\pi}{16} n_{\mathrm{n}} \overline{v}_{\mathrm{n}} \phi_{\mathrm{n}} d_0^2 \tag{34}$$

In this equation, $\overline{v}_{\mathrm{n}}$ denotes the mean thermal velocity of neutral particles, d_0 the discharge chamber's inner diameter, and ϕ_{n} the extraction grids' opening fraction for neutrals. The opening fraction is obtained by relating the extraction hole area to the total grid area.[22] With this information, the mass efficiency of the thruster can be estimated by

$$\eta_m = \frac{\gamma_{\mathrm{i}}}{\gamma_{\mathrm{i}} + \gamma_{\mathrm{n}}}, \tag{35}$$

with $\gamma_{\mathrm{i}} = I_{\mathrm{b}}/e$.

The particle conservation model now predicts the net mass flow leaving the thruster (assuming $m_{\mathrm{i}} \approx m_{\mathrm{n}}$):

$$\dot{m} = \frac{m_{\mathrm{i}} I_{\mathrm{b}}}{e \eta_m} \approx m_{\mathrm{i}} \left(\gamma_{\mathrm{n}} + \gamma_{\mathrm{i}}\right) \tag{36}$$

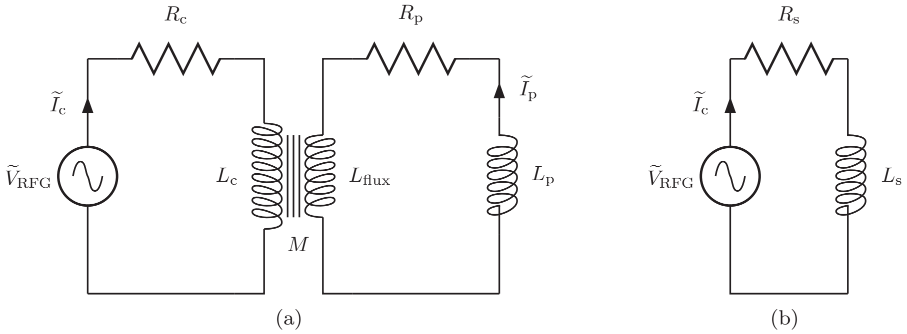

Figure 5. Equivalent circuit of an inductive plasma discharge (a). Effective load seen by the RFG (b).

The corresponding volumetric flow rate in sccm is obtained using the density of the gas ρ:

$$\dot{V}' = 6 \times 10^7 \frac{\dot{m}}{\rho} \tag{37}$$

To close the self-consistent loop the discharge pressure is iteratively updated using a modified version of an conservation equation from Ref. 22:

$$p_{k+1} = p_k \left[1 + \alpha \left(1 - \frac{\dot{V}'_k}{\dot{V}} \right) \right] \tag{38}$$

In this equation, k denotes the actual iteration step, $\dot{V}'_k$ the volumetric flow rate in the k-th iteration, and α a factor which is automatically decremented in case of numerical oscillation.

Since the iterative description of the plasma discharge in the presence of ion and neutral extraction is now brought to convergence, the transformer model is called. Inductive discharges are commonly described by a transformer circuit, as introduced in Ref. 23. As depicted in Fig. 5 (a), the transformer primary represents the RFG attached to the induction coil, resulting in an impedance of $Z_c = R_c + i\omega L_c$. The secondary shows the plasma contributions; i.e., $Z_p = R_p + i\omega \left(L_{flux} + L_p \right)$.

The impedance of the coil alone—which corresponds to the transformer primary—is obtained by a 3D magneto-quasistatic model based on Biot-Savart's law. Detailed information can be found in Refs. 24 and 25. The plasma impedance is given by the energy storage inductance caused by the plasma current L_{flux}, the inductance due to electron inertia L_p, and the plasma resistance R_p. Both circuits are coupled by a mutual inductance M which is obtained using Kirchhoff's law on primary and secondary.[6] The lumped elements calculate to:[5,6,23]

$$R_p = \frac{2 P_{abs}}{\left| \widetilde{I}_p \right|^2} \tag{39}$$

$$L_{flux} = \frac{2 \left(U_{m,0} - U_m \right)}{\left| \widetilde{I}_p \right|^2} \tag{40}$$

$$L_p = \frac{R_p}{\nu_{m,eff}} \tag{41}$$

$$M = \frac{\widetilde{I}_p}{\widetilde{I}_c} \left(\frac{i R_p}{\omega} - \left(L_{flux} - L_p \right) \right) \tag{42}$$

In Eq. (40), $\widetilde{I}_p$ denotes the plasma current and U_m the magnetic energy within the simulation domain. It is obtained by numerical integration of

$$U_m = \frac{1}{4} \iiint_V \mathrm{Re} \left\{ \widetilde{\mathbf{H}} \widetilde{\mathbf{B}}^* \right\} \mathrm{d}V, \tag{43}$$

Table 1. Geometrical parameters of a RIM-4 thruster.

r_c	l_0	N_c	d_c	t_v	d_s	d_a	t_s	N_h	l_g
22.70 mm	41.00 mm	6	3.00 mm	1.25 mm	1.90 mm	1.20 mm	0.50 mm	151	0.75 mm

with magnetic field vector $\widetilde{\mathbf{H}} = \widetilde{\mathbf{B}}/\mu_0$, as given in Ref. 12. Furthermore, $U_{m,0}$ denotes the magnetic energy without the plasma being ignited.

The transformer circuit can be transformed to its series load representation, as depicted in Fig. 5 (b), using circuit theory:[26]

$$R_s = R_c + \omega^2 M^2 \frac{\operatorname{Re} Z_p}{|Z_p|^2} \tag{44}$$

$$L_s = L_c - \omega^2 M^2 \frac{\operatorname{Im} Z_p}{|Z_p|^2} \tag{45}$$

The implementation of the performance model is straight forward since closed-form solutions can be used due to converged plasma and propulsive parameters. First, an energy balance that relates the ions' kinetic energy to their potential energy is solved for the velocity of the accelerated ions leaving the thruster via the extraction system:[1]

$$v_i = \sqrt{\frac{2e\left(V_{acc} - V_{dec}\right)}{m_i}} \tag{46}$$

With Eqs. (28) and (34), the generated thrust is obtained:

$$F = m_i \gamma_i v_i + m_n \gamma_n \overline{v}_n \tag{47}$$

Since neutral particles leaving the thruster hardly contribute to the generated thrust due to low thermal velocity (they are assumed to be thermalized with the wall temperature which is set to 400 K) an effective exhaust velocity v_{eff} is derived:

$$v_{eff} = \frac{F}{\gamma_i m_i + \gamma_n m_n} \tag{48}$$

Based on that, the thruster's specific impulse can be derived as

$$I_{sp} = \frac{v_{eff}}{g}, \tag{49}$$

with g denoting standard gravity.

Both, specific impulse and mass efficiency from Eq. (35) basically describe the thruster's efficiency regarding propellant consumption. However, for finding optimized sets of input parameters the overall efficiency of the thruster has to be considered. For this reason, electrical efficiency is also taken into account. It relates the actual beam power $I_b\left(V_{acc} - V_{dec}\right)$ to the power absorbed in the plasma, given in Eqs. (25) and (26):

$$\eta_{el} = \frac{I_b\left(V_{acc} - V_{dec}\right)}{I_b\left(V_{acc} - V_{dec}\right) + P_{abs}} \tag{50}$$

III. Simulation Results and Verification

A RIM-4 RF ion thruster developed at the University of Giessen is evaluated in this section. The geometrical parameters of the thruster are given in Table 1, with inner coil radius r_c, number of coil windings N_c, coil wire diameter d_c, discharge vessel wall thickness t_v, and acceleration grid hole diameter d_a.

The threshold potentials for xenon used in the simulations are $\mathcal{E}_{ex} = 8.32\,\mathrm{eV}$, $\mathcal{E}_{iz} = 12.13\,\mathrm{eV}$, as given in Ref. 9. According to Ref. 27 the ion-neutral momentum transfer cross section approximates to $\sigma_{in} \approx 8.20872 \times 10^{-16}\,\mathrm{m}^3/\overline{v}_r\,\mathrm{s}$, with a relative velocity between incident ions and neutral background gas of $\overline{v}_r = \left(16e\mathrm{T}_n/\pi m_i\right)^{1/2}$, taking reduced mass $m_r = m_i m_n/\left(m_i + m_n\right) \approx m_i/2$ of the two species into account.

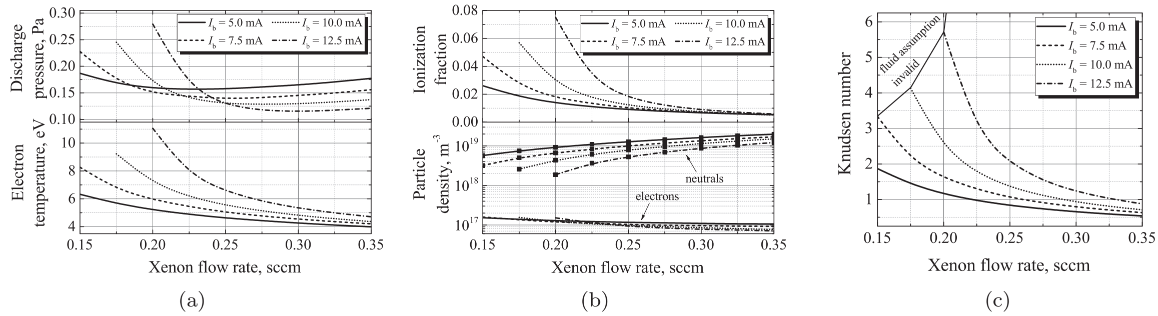

Figure 6. Simulation results showing electron temperature and discharge pressure (a), particle densities and ionization fraction (b), and the Knudsen number to estimate the validity of the fluid assumption (c).

Figure 6 (a) shows the electron temperature and the discharge pressure with respect to the volumetric xenon flow rate for different extracted ion beam currents. The discharge pressure curves go through a minimum because at lower flow rates electron temperature as well as ionization fraction (cf. Fig. 6 (b)) increase, leading to an increase in pressure according to Eq. (4). When going to higher flow rates, electron temperature and ionization fraction asymptotically approach stable values and their influence on the discharge pressure is almost negligible. But the amount of neutral particles entering the system increases, as can be seen in Fig. 6 (b). This again leads to an increase in pressure due to the term related to the neutral particles in Eq. (4). Their influence is weaker than that of the electrons. Hence, the minimum is stretched and shifted depending on the amount of extracted ion beam current. The simulations are unstable for constellations of high extracted current and low volumetric flow rates. This is due to an increasing Knudsen number,

$$\mathrm{Kn} = \frac{\lambda_{\mathrm{in}}}{l_{\mathrm{char}}}, \tag{51}$$

that relates the mean free path of the most infrequent modeled collision process λ_{in}; i.e., ion-neutral collisions, to the characteristic length between collisions l_{char}. With this functionality, a worst-case scenario is defined that predicts the validity of the fluid assumption. According to Ref. 28 fluid assumptions are generally regarded valid up to $\mathrm{Kn} \leq 0.1$, but sometimes yield useful output in the area $\mathrm{Kn} < 10$. In the latter case, experimental verification of the output is inevitable which is shown below. The corresponding Knudsen numbers of each simulated data point are shown in Fig. 6 (c). The simulations have been performed for a fixed radio-frequency of $f = 2.4\,\mathrm{MHz}$ and fixed extraction voltages of $V_{\mathrm{acc}} = 1400\,\mathrm{V}$ with $V_{\mathrm{dec}} = 150\,\mathrm{V}$.

The electric field and absorbed power density distribution are shown in Fig. 7 (a) and (b), respectively. The field plots correspond to a coil current of $\widetilde{I}_{\mathrm{c}} = I_{\mathrm{c}} = 5.28\,\mathrm{A}$; i.e., a purely sinusoidal current with no starting phase, a volumetric xenon flow rate of $\dot{V} = 0.15\,\mathrm{sccm}$, and 116^3 Cartesian mesh nodes within the simulation domain. It can be seen that effective plasma heating only occurs near the walls of the discharge chamber. This is partly due to the skin effect and partly due to geometrical properties of the solenoidal induction coil.

After application of Eqs. (25) and (39) – (45) the volume-averaged electrical discharge parameters are obtained. The series-transformed thruster impedance magnitude $|Z_{\mathrm{s}}| = \left(R_{\mathrm{s}}^2 + L_{\mathrm{s}}^2\right)^{1/2}$, resistance R_{s}, and inductance L_{s} are shown in Fig. 8 (a). As can be seen, the change of impedance with respect to flow rate and extracted ion current is comparably low. This is due to the inverse behavior of R_{s} and L_{s}. In order to develop control mechanisms (e.g. for the RFG's matching unit) it is highly desirable to know the dynamic behavior of the resistive and reactive components. With the model proposed, this behavior can be obtained for arbitrary constellations of input parameter sets.

Figure 8 (b) shows a performance map of the thruster that relates total RFG power to propellant flow rate and extracted ion current. With constant RFG and cable loss assumed, the simulated lines are in good agreement with values obtained experimentally. As mentioned earlier, the model's output loses reliability for constellations of low flow rate and high extracted current due to the decreasing validity of the fluid assumption.

The thruster's performance data is shown in Fig. 9. Graph (a) shows deliverable thrust and specific

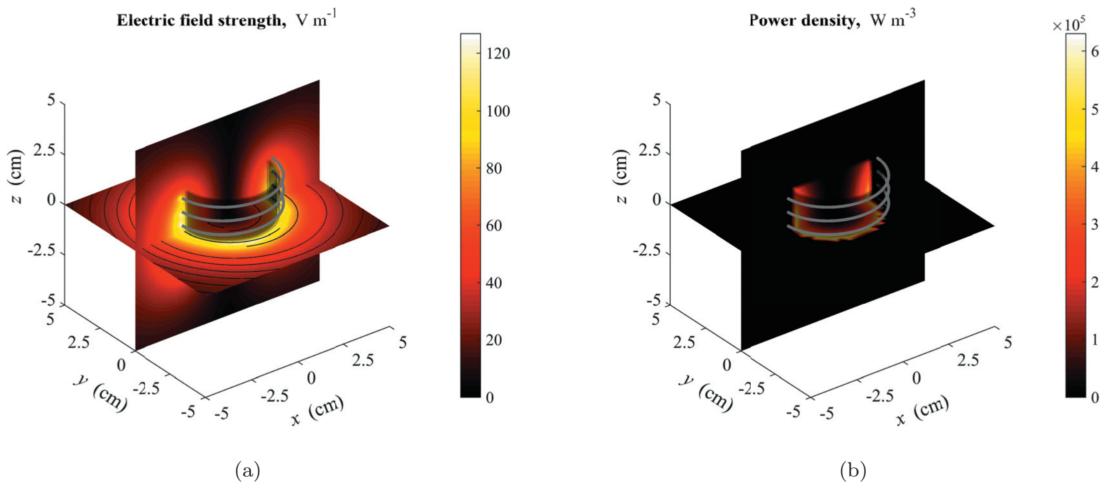

Figure 7. Simulated magnitudes and streamlines for electric field (a) and simulated magnitudes of the absorbed power density (b).

impulse and graph (b) shows mass, electrical, and overall thruster efficiency. The thrust is kept constant using a software PI controller that controls the extracted beam current by adjusting the coil current with respect to flow rate. For high extraction currents fairly high specific impulse is obtainable ($> 3000\,\mathrm{s}$). Specific impulse and mass efficiency show basically the same behavior since they both evaluate the amount of consumed propellant to sustain a certain amount of thrust. In contrast to that, the electrical efficiency shows an almost inverted behavior and increases with increasing flow rate and extracted current. This results in an overall thruster efficiency that reaches a maximum at a certain flow rate (for each extracted current; i.e., delivered thrust). Since those areas with maximum efficiency—which are relevant for space missions—can be resolved with the proposed model and its predictive power, it can be considered an extremely valuable toolbox for engineering purposes.

IV. Conclusions

In this paper we introduced a self-consistent 1D/3D hybrid model that predicts electrical characteristics as well as propulsive performance parameters of gridded RF-ion thrusters. A 3D electromagnetic field solver that works in the quasi-stationary regime solves the magnetic diffusion equation on a Cartesian simulation grid. The plasma parameters are coupled to the fields within the diffusion equation in terms of a complex conductivity. The data describing the plasma was obtained using fluid equations within the Uniform Density Discharge Model introduced in Ref. 5. The combination of 3D electromagnetic field solver and 1D plasma solver offers the opportunity of fast simulation duration and physically correct solutions. To prove this, a theoretical performance map of a RIM-4 thruster was obtained using the model and compared with experimentally obtained values, yielding a good agreement.

Due to its 3D core, the model is capable of accounting for arbitrary coil and discharge chamber geometries. Together with its ability of parameter-sweeping input parameters like coil current, radio-frequency, extraction voltages, and volumetric propellant flow rate, this model can be used to find optimal parameter sets and geometrical relations to achieve a highly efficient discharge.

Acknowledgments

We thank Kristof Holste from the University of Giessen for his cooperation. Further, we thank Martin Becker and Patrick Dietz from the University of Giessen for conducting experiments to obtain the measured thruster performance data. This work was partially supported in the framework of LOEWE-Schwerpunkt RITSAT by the Hessian State Ministry of Higher Education, Research and the Arts (HMWK).

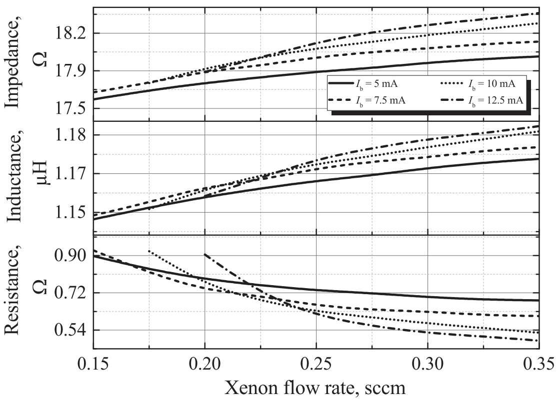

(a)

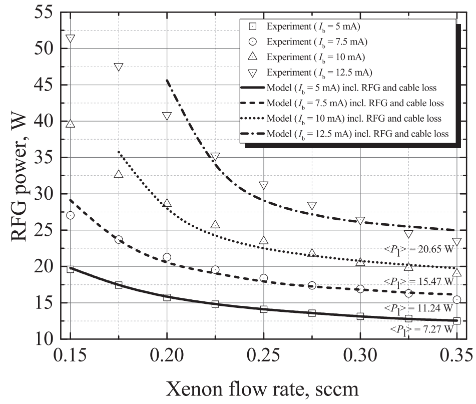

(b)

Figure 8. Volume-averaged electrical parameters of the thruster (a) and performance map for verification (b).

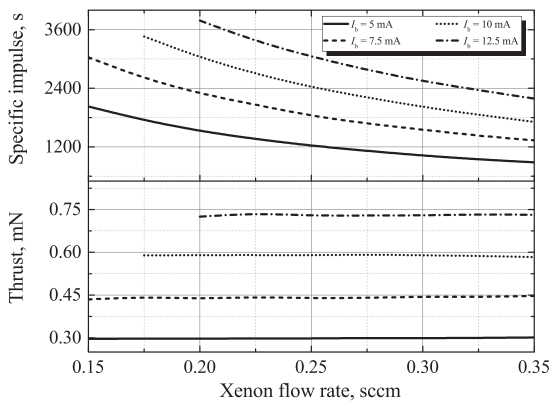

(a)

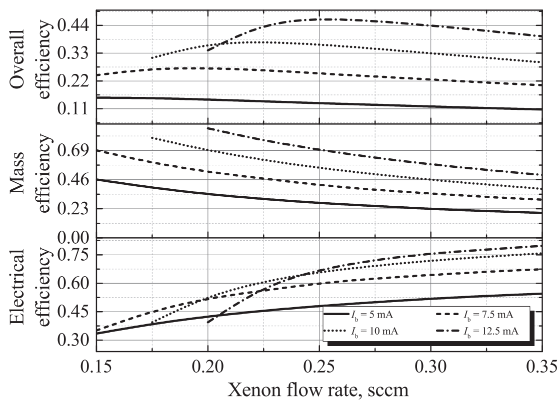

(b)

Figure 9. Thrust and specific impulse (a) and mass, electrical, and overall thruster efficiency (b).

References

[1]Goebel, D. M. and Katz, I., *Fundamentals of Electric Propulsion: Ion and Hall Thrusters*, John Wiley & Sons, 2008.

[2]Ley, W. (ed.), Wittmann, K. (ed.), and Hallmann, W. (ed.), *Handbook of Space Technology*, John Wiley & Sons, 2009.

[3]Killinger, R., Kukies, R., Surauer, M., Tomasetto, A., and van Holtz, L., "ARTEMIS orbit raising inflight experience with ion propulsion", *Acta Astronautica*, Vol. 53, No. 4, 2003, pp. 607-621.

[4]Volkmar, C. and Ricklefs, U., "Implementation and verification of a self-consistent 1D/3D hybrid performance and impedance model of gridded radio-frequency ion thrusters", *European Physical Journal D* (to be published).

[5]Lieberman, M. A. and Lichtenberg, A. J., *Principles of Plasma Discharges and Materials Processing*, 2nd edn., John Wiley & Sons, 2005.

[6]Chabert, P. and Braithwaite, N., *Physics of Radio-Frequency Plasmas*, Cambridge University Press, 2011.

[7]Bronshtein, I. N., Semendyayev, K. A., Musiol, G., and Muehlig, H., *Handbook of Mathematics*, 5th

edn., Springer, 2007.

[8]Lee, C. and Lieberman, M. A., "Global model of Ar, O_2, Cl_2, and Ar/O_2 high-density plasma discharges", *Journal of Vacuum Science & Technology A*, Vol. 13, No. 2, 1995, pp. 368-380.

[9]Hayashi, M., "Bibliography of electron and photon cross sections with atoms and molecules published in the 20$^{\mathrm{th}}$ century – xenon –", NIFS-DATA-79, 2003.

[10]Hayashi database, http://www.lxcat.net [cited 6 May 2015].

[11]Huba, J. D., "NRL plasma formulary", The Office of Naval Research, 2007.

[12]Jackson, J. D., *Classical Electrodynamics*, 3rd edn., John Wiley & Sons, 1998.

[13]Turkoz, E. and Celik, M., "2-D electromagnetic and fluid models for inductively coupled plasma for RF ion thruster performance evaluation", *IEEE Transactions on Plasma Science*, Vol. 42, No. 1, 2014, pp. 235-240.

[14]Chabert, P, Arancibia Monreal, J., Bredin, J, Popelier, L, and Aanesland, A., "Global model of a gridded-ion thruster powered by a radiofrequency inductive coil", *Physics of Plasmas*, Vol. 19, No. 7, 2012, p. 073512.

[15]Goebel, D. M., "Analytical discharge model for RF ion thrusters", *IEEE Transactions on Plasma Science*, Vol. 36, No. 5, 2008, pp. 2111-2121.

[16]Tsay, M. M. and Martinez-Sanchez, M., "Simple performance modeling of a radio-frequency ion thruster", *Proceedings of the 30th International Electric Propulsion Conference*, Florence, Italy, 2007, Proceeding IEPC-2007-072.

[17]Sadiku, M. N. O., *Numerical Techniques in Electromagnetics*, 2nd edn., CRC-Press, 2000.

[18]Yang, S. and Gobbert, M. K., "The optimal relaxation parameter for the SOR method applied to the Poisson equation in any space dimensions", *Applied Mathematics Letters*, Vol. 22, No. 3, 2009, pp. 325-331.

[19]Mitchner, M. and Kruger, C. H., *Partially Ionized Gases*, John Wiley & Sons, 1973.

[20]Rovang, D. C. and Wilbur, P. J., "Ion extraction capabilities of closely spaced grids", *Proceedings of the AIAA/JSASS/DGLR 16th International Electric Propulsion Conference*, New Orleans, USA, 1982, Proceeding AIAA-82-1894.

[21]Rovang, D. C. and Wilbur, P. J., "Ion extraction capabilities of two-grid accelerator systems", *Journal of Propulsion and Power*, Vol. 1, No. 3, 1985, pp. 172-179.

[22]Tsay, M. M., "Numerical modeling of a radio-frequency micro ion thruster", Master's thesis, Department of Aeronautics and Astronautics, Massachusetts Institute of Technology, Cambridge, MA, USA, 2006.

[23]Piejak, R. B., Godyak, V. A., and Alexandrovich, B. M., "A simple analysis of an inductive RF discharge", *Plasma Sources Science and Technology*, Vol. 1, No. 3, 1992, pp. 179-186.

[24]Volkmar, C., Baruth, T., Simon, J., Ricklefs, U., and Thueringer, R., "Arbitrarily shaped coils' inductance simulation based on a 3-dimensional solution of the Biot-Savart law", *Proceedings of the 36th International Spring Seminar on Electronics Technology*, Alba Iulia, Romania, 2013, pp. 210-215.

[25]Volkmar, C., Simon, J., and Ricklefs, U., "Numerical determination of induced electric eddy fields inside arbitrarily shaped induction coils", *Journal of Physical Science and Application*, Vol. 4, No. 4, 2014, pp. 262-268.

[26]Terman, F. E., *Radio Engineer's Handbook*, McGraw-Hill, 1943.

[27]Banks, P., "Collision frequencies and energy transfer — electrons", *Planetary and Space Science*, Vol. 14, No. 11, 1966, pp. 1085-1103.

[28]Anderson, J. D., *Computational Fluid Dynamics*, McGraw-Hill, 1995.